Received 23 May 2021; revised 19 June 2021; accepted 19 June 2021. Date of publication 22 June 2021; date of current version 6 July 2021.

Digital Object Identifier 10.1109/OJCOMS.2021.3091606

Hardware and Interference Limited Cooperative CR-NOMA Networks Under Imperfect SIC and CSI

SULTANGALI ARZYKULOV [1] (Member, IEEE), GALYMZHAN NAURYZBAYEV [2] (Senior Member, IEEE), ABDULKADIR CELIK [1] (Senior Member, IEEE), AND AHMED M. ELTAWIL [1] (Senior Member, IEEE)

[1]Computer, Electrical and Mathematical Science and Engineering Division, King Abdullah University of Science and Technology, Thuwal 23955-6900, Saudi Arabia

[2]Department of Electrical and Computer Engineering, Nazarbayev University, Nur-Sultan 010000, Kazakhstan

CORRESPONDING AUTHOR: S. ARZYKULOV (e-mail: sultangali.arzykulov@kaust.edu.sa)

This work was supported in part by the King Abdullah University of Science and Technology (KAUST), in part by the Communication and Computing Systems Lab, and in part by the Nazarbayev University Faculty Development Competitive Research Program under Grant 240919FD3935.

This work did not involve human subjects or animals in its research.

ABSTRACT The conflation of cognitive radio (CR) and non-orthogonal multiple access (NOMA) concepts is a promising approach to fulfill the massive connectivity goals of future networks given the spectrum scarcity. Accordingly, this paper investigates the performance of a cooperative CR-NOMA network in the presence of system impairments and interference. Our analysis is involved with the derivation of the end-to-end outage probability for primary and secondary networks by accounting for channel state information (CSI), hardware imperfections, and residual interference caused by successive interference cancellation errors as well as coexisting primary/secondary users. Moreover, a mathematically tractable upper bound on spectral efficiency (SE) with its high-SNR approximations are derived. Besides, we propose an optimal power allocation scheme for CR-NOMA users to guarantee their outage and SE fairness. The numerical results validated by Monte Carlo simulations show that the CR-NOMA network provides a superior outage performance over orthogonal multiple access. Furthermore, the higher level of system imperfections leads to the performance degradation of the CR-NOMA networks. As imperfections become more severe, the CR-NOMA is observed to deliver relatively inferior outage and SE performance as compared to the perfect system scenario.

INDEX TERMS Cognitive radio, cooperative non-orthogonal multiple access, outage probability (OP), spectral efficiency, hardware impairment.

I. INTRODUCTION

THE AMBITIOUS quality-of-service (QoS) demands of future wireless networks pose daunting challenges, especially under the ever-increasing number of devices connected to the Internet [1]. This consequently leads to two problems: spectrum scarcity and interference-limited networks. The spectrum scarcity has been mostly studied in the realm of cognitive radio (CR) networks. The CR is aimed to provide communication for secondary users (SUs) over the spectrum bands of licensed users (a.k.a. primary users (PUs)) [2]. The most prevalent CR paradigm is the underlay CR, where SUs can regularly use primary spectrum bands. However, secondary transmit nodes should transmit below the interference tolerance level of primary receivers to avoid causing harmful interference to the primary network (PN) [3], [4]. Moreover, considering the underlay CR's transmission power limitation, the relaying technique can be used to extend its communication link. Alternatively, non-orthogonal multiple access (NOMA) schemes have also recently received attention as a promising technique to mitigate the limitation of orthogonal multiple access (OMA) schemes in supporting massive connectivity [5]. The NOMA's fundamental concept is to allow users to share the same radio resource by transmitting signals of users in a superposition manner and implementing successive interference cancellation (SIC) at the receivers' end [6]. The most popular NOMA scheme is the power domain NOMA, where a transmit node simultaneously sends messages for all intended users by assigning different power levels depending on the users' channel states or service priority [7].

II. RELATED WORKS

The conflation of CR and NOMA concepts (CR-NOMA) is regarded as a potential solution to efficient spectrum utilization in massively connected wireless networks. For instance, [8] studied the underlay CR-NOMA to improve the secondary network's (SN) connectivity. As a result, it was concluded that NOMA can outperform OMA if the target rate and power allocation (PA) factors are properly designed. The overlay CR-NOMA was examined in [9], where SUs exploiting the NOMA protocol can convey their signals over the primary frequency band and help relay primary signals to their destination users. The advantage of the relaying technique has also been utilized in CR-NOMA networks. In the underlay CR, short-range relaying communication can enhance the performance of power-restricted SNs [3], [10]. Besides, the throughput and coverage area can also be improved with the aid of a relaying station [11]. The author in [10] introduced a new cooperative multicast CR-NOMA, where SUs' fairness is improved by applying a two-stage cooperative scheme. Besides, in [12], it was proved that utilizing the cooperative method in the CR networks contributes to notable performance in terms of inter-cell interference improvements.

There are other existing literature on cooperative CR-NOMA networks [13]–[16]. For example, Kumar *et al.* studied the sum rate and outage probability (OP) of an underlay relaying CR-NOMA [13], where they showed that the CR-NOMA system performs better than the CR-OMA one. A cognitive NOMA scheme where the strong user performs spectrum sensing was studied by Jia *et al.* [14]. The authors studied the OP and throughput for the considered system model taking into account delay-limited and delay-tolerant transmission modes. Furthermore, Wang *et al.* studied full-duplex CR-NOMA networks [16], where numerical results showed that the proposed model outperforms the half-duplex model if proper self-interference cancellation is executed. Moreover, Yue *et al.* and Lei *et al.* studied the downlink NOMA systems in terms of the relationship between reliability and security [17], [18]. The authors in [19] presented the performance analysis of a downlink underlay CR-NOMA system, where closed-form expressions for the outage probability and average achievable sum-rate of the SUs were derived considering various scenarios of the CSI availability.

The literature mentioned above on cooperative CR-NOMA networks mostly deals with simple scenarios under ideal cases without paying sufficient attention to practical limitations. In practice, all transceivers undergo several hardware impairments (HIs) [20]. Some residual transceiver HIs produced by inexact calibration and different sorts of noise can not be appropriately removed despite the existence of various algorithms designed to mitigate HIs' impact [21]. Björnson *et al.* demonstrated that the effect of HIs on system performance can not be eliminated by manipulating the transmit power [22]. Moreover, Selim *et al.* demonstrated the influence of HIs on NOMA systems [23]. In addition to HIs, in practical NOMA networks, it is highly idealistic to consider the perfect SIC detection [24]. Hence, there is a need to investigate the influence of HIs and imperfect SIC on underlay CR-NOMA networks as they can degrade the system performance in terms of the OP, spectral efficiency (SE), ergodic capacity, etc.

Accordingly, in contrast to [13], [25], [26], where no or only imperfect CSI was considered, this paper investigates the OP of a generalized and imperfect CR-NOMA, where non-ideality is modeled by accounting for practical system limitations such as hardware impairments (HIs), CSI imperfections, and residual interference caused by error propagation during SIC. Moreover, different from [4], where the system was studied by neglecting the effect of the additive white Gaussian noise (AWGN), we study interference- and noise-limited CR-NOMA network with aforementioned system limitations. Moreover, while [4] considered the fixed PA factors, we propose an algorithm to find optimal PA factors to guarantee equal outage performance for all NOMA users.

The key contributions of the paper are summarized as:

- We provide exact closed-form equations for the OP of secondary and primary CR-NOMA users considering practical system limitations in terms of HIs, imperfect CSI and SIC. Besides, ensuring that primary traffic is protected, our analysis also tackles the random interference caused by co-existing primary/secondary users.
- To gain a more in-depth insight, we derive a high signal-to-noise-ratio (SNR) approximated OP of the SN for two asymptotic cases. In the first scenario, we derive the OP assuming that the SN is not restricted by the maximum transmit power, which can be considered as a non-cognitive NOMA network. In the second scenario, we consider that the primary receiver node's interference tolerance level is the dominant factor in determining the maximum allowed transmit power at the SN.
- Furthermore, we develop an algorithm to find optimal power allocated to CR-NOMA users. The algorithm provides optimal PA factors for each NOMA user to guarantee fair OP by considering the practical system constraints.
- Considering the optimal PA, we derive an upper bound on SE and its high SNR approximation expression to provide valuable insights into the effect of each system impairment. Finally, the numerical results validated by Monte Carlo simulations show that the CR-NOMA network provides a superior outage performance over the benchmark OMA one.

The remainder of this paper is organized as follows. Section III introduces the system model and transmission protocol of a downlink CR-NOMA network. Section IV provides and discusses new closed-form and approximated analytical expressions for the OP of SN and PN. In Section V, we discuss an algorithm for finding optimal PA coefficients to provide fair OP for users. Section VI provides analytical derivations of the upper bound on SE and asymptotic high-SNR SE for the proposed system model. Section VII shows numerical findings to validate

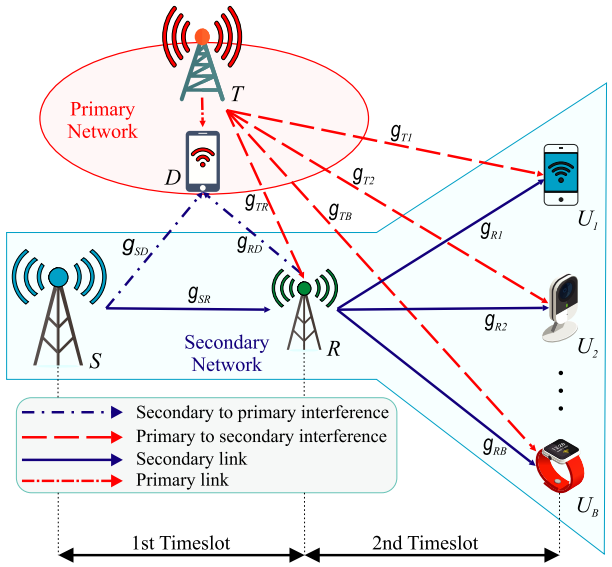

FIGURE 1. The proposed underlay CR-NOMA network.

the correctness of theoretical analysis. Finally, the paper's key findings are summarized in Section VIII.

III. SYSTEM MODEL

We consider a downlink CR-NOMA network that consists of PN and SN as illustrated in Fig. 1. The PN comprises the primary transmitter (T) and destination (D) nodes. On the other hand, the SN consists of a source (S), a relay[1] (R) that cooperates with S in a half-duplex decode-and-forward (DF) mode, and B secondary NOMA users ($U_1, \ldots, U_B$). The cooperation in the SN occurs over two time slots; the broadcast signal transmitted by S in the first time slot is re-transmitted to B NOMA users in the second time slot. Channel gains between the nodes are modeled as $g_i \sim \mathcal{CN}(0,1)$, $\forall i \in \{SD, SR, RD, R1, \ldots, RB, TR, T1, \ldots, TB\}$. Moreover, the distance between the corresponding nodes and the path-loss exponent are denoted by d_i and τ, respectively. To capture the CSI imperfections, we model channel coefficients using a minimum mean square error channel estimator as

$$g_i = h_i + e_i, \tag{1}$$

where $h_i \sim \mathcal{CN}(0, \sigma_{h_i}^2)$ and $e_i \sim \mathcal{CN}(0, \zeta_i)$ are the estimated channel coefficient and channel estimation error, respectively, with $\sqrt{\sigma_{h_i}^2 + \zeta_i} = 1$. The error variance is modeled as $\zeta_i \triangleq \theta\rho^{-\kappa}$, where $\rho = \frac{P}{\sigma^2}$ is the transmitted SNR, and $\kappa \geq 0, \theta > 0$ [27]. Indeed, this model describes various CSI acquisition scenarios: a) ζ is a function of ρ for $\kappa \neq 0$, and b) ζ is independent of ρ for $\kappa = 0$. Following from the underlay CR paradigm, the QoS of the PN is considered tolerable if the interference from the SN is below a given interference temperature constraint (ITC). Therefore, we assume that the transmit power of node j, $j \in \{R, S\}$, is restricted as

$$P_j \leq \min\left(P_{\max}, \frac{I_{\text{ITC},j}\, d_{jD}^{\tau}}{\left|g_{jD}\right|^2}\right), \tag{2}$$

where $P_{\max}$ stands for the maximum transmit power at node j and $I_{\text{ITC},j}$ denotes the ITC at D caused by node j.

A. TRANSMISSION PROTOCOL FOR SECONDARY NETWORK

In the first time slot, S broadcasts $\sum_{b=1}^{B}\sqrt{\alpha_b}x_b$ to R, where α_b is the PA factor[2] of U_b and $\sum_{b=1}^{B}\alpha_b = 1$, and x_b is the message dedicated to U_b, with $\mathbb{E}(|x_b|^2) = 1$. Considering the CSI imperfections and aggregate distortion noise, the received signal at R can be written as

$$y_R = \left(h_{SR} + e_{SR}\right)\sqrt{\bar{P}_S}\left(\sum_{b=1}^{B}\sqrt{\alpha_b}x_b + \eta_{SR}\right) + g_{TR}\sqrt{\bar{P}_T}\left(x_T + \eta_{TR}\right) + n_R, \tag{3}$$

where $\bar{P}_i = \frac{P_i}{d_{iR}^{\tau}}$, $i \in \{S, T\}$; $\eta_{(\cdot)} \sim \mathcal{CN}(0, \phi_{(\cdot)}^2)$ denotes the aggregate distortion noise from transceiver; $\phi_{(\cdot)} = \sqrt{\phi_t^2 + \phi_r^2}$ is the aggregate HI level from a transmitter and receiver [31]; $n_{(\cdot)} \sim \mathcal{CN}(0, \sigma_{(\cdot)}^2)$ denotes the AWGN term at each receiver node; P_T and x_T stand for the transmit power at T and the message dedicated to D, respectively. Then, the instantaneous signal-to-interference-distortion-noise-ratio (SIDNR) to decode x_b, $1 \leq b < B$, at R can be expressed by

$$\gamma_{R,b} = \frac{\alpha_b\left|h_{SR}\right|^2}{(I_{Rb} + \phi_{SR}^2)\left|h_{SR}\right|^2 + C_R + I_{TR}\left|g_{TR}\right|^2 + \delta_R}, \tag{4}$$

where

$$I_{Rb} = \sum_{m=b+1}^{B}\alpha_m + \sum_{n=1}^{b-1}\vartheta_n\,\alpha_n, \tag{5}$$

where the first summation in (5) is the non-removable interference of the weaker users, while the second term is the residual interference caused by the SIC inefficiency,[3] with $0 \leq \vartheta_n \leq 1$. The channel error plus hardware distortion noise power is denoted by $C_R = \zeta_{SR} + \zeta_{SR}\phi_{SR}^2$ and the interference

1. R can be a small base station that is the part of secondary architecture and the purpose of which is to extend the coverage range of the SN.

2. There are two main ways of ordering the NOMA users in the available literature. The first method orders the NOMA nodes according to their channel statistics. In other words, the message of a user with the weakest channel state is decoded first [26], [28]. In the second method, the users are sorted according to their QoS priorities and the user with the higher QoS priority is allocated with higher transmission power [29], [30]. The user ordering according to their QoS is a more realistic and reasonable assumption, since, in real-time communication, it is very likely that NOMA users can have similar channel quality. Thus, in this paper, we consider channel ordering on users' QoS and PA factors are ordered as $\alpha_1 > \ldots > \alpha_b > \ldots > \alpha_B$.

3. This SIC error model serves as the worst-case scenario by providing a lower bound performance on any practical NOMA-based scenario [32]. However, there are other SIC models where the error is a discrete RV according to constellations [33], which are beyond the scope of the paper.

received from T is given by $I_{TR} = \frac{\bar{P}_T}{\bar{P}_S}(1+\phi_{TR}^2)$. Finally, $\delta_R = \frac{\sigma_R^2}{\bar{P}_S}$ is the normalized thermal noise at R. Furthermore, by assuming the imperfect detection of x_b, R decodes the message of user B with the SIDNR of

$$\gamma_{R,B} = \frac{\alpha_B |h_{SR}|^2}{I_{RB}|h_{SR}|^2 + \phi_{SR}^2|h_{SR}|^2 + C_R + I_{TR}|g_{TR}|^2 + \delta_R}, \quad (6)$$

where $I_{RB} = \sum_{n=1}^{B-1} \Im_n \alpha_n$ is the residual interference caused by the SIC inefficiency.

In the second time slot, R relays the decoded signal $\sum_{b=1}^{B}\sqrt{\beta_b}\tilde{x}_b$ to B NOMA users, where β_b, with $\sum_{b=1}^{B}\beta_b = 1$, is the PA factor of U_b. Hence, the received signal at U_b is

$$y_b = (h_{Rb} + e_{Rb})\sqrt{\bar{P}_R}\left(\sum_{b=1}^{B}\sqrt{\beta_b}\tilde{x}_b + \eta_{Rb}\right) + g_{Tb}\sqrt{\bar{P}_T}(x_T + \eta_{TR}) + n_b, \quad (7)$$

where $\bar{P}_i = \frac{P_i}{d_{ib}^{\tau}}$, $i \in \{R, T\}$. Then, we can write the SIDNR for U_b to detect the message of U_j as follows

$$\gamma_{b,j} = \frac{\beta_j |h_{Rb}|^2}{I_{bj}|h_{Rb}|^2 + \phi_{Rb}^2|h_{Rb}|^2 + C_b + I_{Tb}|g_{Tb}|^2 + \delta_b}, \quad (8)$$

where $1 \le j \le b < B$, $\beta_1 > \beta_j > \beta_b > \beta_B$, and

$$I_{bj} = \sum_{m=j+1}^{b}\beta_m + \sum_{m=1}^{j-1}\Im_m \beta_m \quad (9)$$

denotes the interference caused by the weaker users' messages and SIC inefficiency. The channel error plus hardware distortion noise power is denoted by $C_b = \zeta_{Rb} + \zeta_{Rb}\phi_{Rb}^2$ and the PN interference is given by $I_{Tb} = \frac{\bar{P}_T}{\bar{P}_R}(1+\phi_{Tb}^2)$. Lastly, $\delta_b = \frac{\sigma_b^2}{\bar{P}_R}$ is the normalized thermal noise at U_b. Finally, after decoding messages of $(B-1)$ NOMA users, U_B detects its message using

$$\gamma_B = \frac{\beta_B |h_{RB}|^2}{I_B|h_{RB}|^2 + \phi_{RB}^2|h_{RB}|^2 + C_B + I_{TB}|g_{TB}|^2 + \delta_B}, \quad (10)$$

where $I_B = \sum_{n=1}^{B-1}\Im_n \beta_n$ is the residual interference caused by SIC inefficiency; $C_B = \zeta_{RB} + \zeta_{RB}\phi_{RB}^2$ is the channel error plus hardware distortion noise power; $I_{TB} = \frac{\bar{P}_T}{\bar{P}_R}(1+\phi_{TB}^2)$ denotes the PN interference. Finally, $\delta_B = \frac{\sigma_B^2}{\bar{P}_R}$ is the normalized thermal noise at U_B.

Now, considering the single and dual-hop communication of the PN and SN, accordingly, the respective achievable rates at D and U_b are calculated as

$$\mathcal{R}_D = \mathcal{W}\log_2[1+\gamma_D], \quad (11a)$$

$$\mathcal{R}_b = \frac{\mathcal{W}}{2}\log_2[1+\min(\gamma_{R,b}, \gamma_{b,b})], \ 1 \le b \le B, \quad (11b)$$

where the factor $\frac{1}{2}$ implies the two time slots over which the end-to-end communication takes place, and $\mathcal{W}$ is the available bandwidth and $\gamma_{b,b}$ is the SIDNR for U_b when $j = b$ in (8).

IV. OUTAGE ANALYSIS

A. OUTAGE FOR SECONDARY NETWORK

The outage at U_b occurs when the achievable rate at U_b is below a predefined rate threshold $\mathcal{R}_{\text{th},b}$. Following from (11b), the OP of U_b can be written as

$$P_{\text{out}}^b = \Pr\left[\frac{1}{2}\log_2[1+\min(\gamma_{R,b}, \gamma_{b,b})] < \mathcal{R}_{\text{th},j}\right] = 1 - \Pr[\min(\gamma_{R,b}, \gamma_{b,b}) > \psi_j] = F_{\gamma_{R,b}}(\psi_b) + F_{\gamma_{b,b}}(\psi_b) - F_{\gamma_{R,b}}(\psi_b)F_{\gamma_{b,b}}(\psi_b), \quad (12)$$

where $\psi_b = 2^{2\mathcal{R}_{\text{th},b}} - 1$ denotes the predefined SNR threshold at U_b. Now, considering the ITC, we can write the cumulative distribution function (CDF) of the random variable (RV) $\gamma_{R,b}$ as in (13), at the bottom of the page, where $X = |h_{SR}|^2$, $Y = |g_{SD}|^2$, and $Z = |g_{TR}|^2$ follow the exponential distribution; $\mathcal{A} = \alpha_b - I_{Rb}\psi_b - \phi_{SR}\psi_b$; $\mathcal{K} = \frac{I_{TR}\psi_b}{\mathcal{A}}$; $\mathcal{M} = \frac{\delta_b\psi_b}{\mathcal{A}}$; $\mathcal{L} = \frac{C_R\psi_b}{\mathcal{A}}$; $\bar{I}_{TR} = \frac{\bar{P}_T d_{SR}^{\tau}(1+\phi_{SR}^2)}{I_{\text{ITC}} d_{SD}^{\tau}}$; $\bar{\delta}_R = \frac{\sigma_R^2 d_{SR}^{\tau}}{I_{\text{ITC}} d_{SD}^{\tau}}$; $\overline{\mathcal{K}} = \frac{\bar{I}_{TR}\psi_b}{\mathcal{A}}$; $\overline{\mathcal{M}} = \frac{\bar{\delta}_R\psi_b}{\mathcal{A}}$ and $\Lambda_S = \frac{I_{\text{ITC}} d_{SD}^{\tau}}{\bar{P}_S}$.

Proposition 1: The CDF of $\gamma_{R,b}$ can be written in its closed-form as follows

$$F_{\gamma_{R,b}}(\psi_b) = 1 - \frac{1-e^{-\Lambda_S}}{e^{\mathcal{M}+\mathcal{L}}(\mathcal{K}+1)} + \frac{\text{Ei}[-\mu_S\xi_S]e^{\mu_S\xi_S}}{\overline{\mathcal{K}}e^{\Lambda_S(1+\overline{\mathcal{M}})+\mathcal{L}}}, \quad (14)$$

where $\mu_S = 1 + \Lambda_S\overline{\mathcal{K}}$, $\xi_S = \frac{\overline{\mathcal{M}}+1}{\overline{\mathcal{K}}}$ and $\text{Ei}[\cdot]$ is the exponential integral function [34, Eq. (8.211)]

Proof: Full proof is relegated in Appendix A. ■

Following from (8), the CDF of $\gamma_{b,b}$ can be described as

$$F_{\gamma_{b,b}}(\psi_j) = \Pr[Q < W\mathcal{S} + \mathcal{O} + \mathcal{T}, V < \Lambda_R] + \Pr[Q < WV\overline{\mathcal{S}} + V\overline{\mathcal{O}} + \mathcal{T}, V > \Lambda_R], \quad (15)$$

where $Q = |h_{Rb}|^2$; $V = |g_{RD}|^2$; $W = |g_{Tb}|^2$; $\mathcal{B} = \beta_b - I_{bb}\psi_b - \phi_{Rb}\psi_b$; $\mathcal{S} = \frac{I_{Tb}\psi_b}{\mathcal{B}}$; $\mathcal{O} = \frac{\delta_b\psi_b}{\mathcal{B}}$; $\mathcal{T} = \frac{C_b\psi_b}{\mathcal{B}}$; $\bar{I}_{Tb} =$

$$F_{\gamma_{R,b}}(\psi_b) = \Pr\left[\frac{\alpha_b|h_{SR}|^2}{(I_{Rb}+\phi_{SR}^2)|h_{SR}|^2 + C_R + I_{TR}|g_{TR}|^2 + \delta_R} < \psi_b, \ P_S < \frac{I_{\text{ITC}} d_{SD}^{\tau}}{|g_{SD}|^2}\right] + \Pr\left[\frac{\alpha_b|h_{SR}|^2}{(I_{Rb}+\phi_{SR}^2)|h_{SR}|^2 + C_R + \bar{I}_{TR}|g_{SD}|^2|g_{TR}|^2 + \bar{\delta}_R|g_{SD}|^2} < \psi_b, \ P_S > \frac{I_{\text{ITC}} d_{SD}^{\tau}}{|g_{SD}|^2}\right] = \underbrace{\Pr[X < Z\mathcal{K} + \mathcal{M} + \mathcal{L}, Y < \Lambda_S]}_{\Delta} + \underbrace{\Pr[X < ZY\overline{\mathcal{K}} + Y\overline{\mathcal{M}} + \mathcal{L}, Y > \Lambda_S]}_{\Upsilon} \quad (13)$$

$\frac{\bar{P}_T d_{Rb}^{\tau}(1+\phi_{Rb}^2)}{I_{\text{ITC}} d_{RD}^{\tau}}$; $\bar{\delta}_b = \frac{\sigma_b^2 d_{Rb}^{\tau}}{I_{\text{ITC}} d_{RD}^{\tau}}$; $\overline{\mathcal{S}} = \frac{\bar{I}_{Tb}\psi_b}{\mathcal{B}}$; $\overline{\mathcal{O}} = \frac{\bar{\delta}_b \psi_b}{\mathcal{B}}$ and $\Lambda_R = \frac{I_{\text{ITC}} d_{RD}^{\tau}}{\bar{P}_R}$. Then, following the approach as in Appendix A, the closed-form CDF expression of $\gamma_{b,b}$ can be written as

$$F_{\gamma_{b,b}}(\psi_b) = 1 - \frac{1 - e^{-\Lambda_R}}{e^{\mathcal{O}+\mathcal{T}}(\mathcal{S}+1)} + \frac{\text{Ei}\left[-\mu_R \xi_R\right] e^{\mu_R \xi_R}}{\overline{\mathcal{S}} e^{\Lambda_R\left(1+\overline{\mathcal{O}}\right)+\mathcal{T}}}, \quad (16)$$

where $\psi_b < \frac{\beta_b}{I_{bb}+\phi_{Rb}^2}$, otherwise, $F_{\gamma_{b,b}}(\psi_b) \sim 1$.

Lastly, the exact OP of U_b can be derived after substituting (14) and (16) into (12) and written as

$$P_{\text{out}}^{b} = 1 - \left(\frac{1 - e^{-\Lambda_S}}{e^{\mathcal{M}+\mathcal{L}}(\mathcal{K}+1)} - \frac{\text{Ei}\left[-\mu_S \xi_S\right] e^{\mu_S \xi_S}}{\overline{\mathcal{K}} e^{\Lambda_S\left(1+\overline{\mathcal{M}}\right)+\mathcal{L}}} \right) \times \left(\frac{1 - e^{-\Lambda_R}}{e^{\mathcal{O}+\mathcal{T}}(\mathcal{S}+1)} - \frac{\text{Ei}\left[-\mu_R \xi_R\right] e^{\mu_R \xi_R}}{\overline{\mathcal{S}} e^{\Lambda_R\left(1+\overline{\mathcal{O}}\right)+\mathcal{T}}} \right). \quad (17)$$

Further, using the achievable rate in (11) and OP equations, the average throughput of U_l, $\forall l \in \{D, b\}$ can be calculated as

$$\text{Th}_l = \mathcal{R}_l \left(1 - P_{\text{out}}^{l}\right). \quad (18)$$

B. ASYMPTOTIC OUTAGE FOR SECONDARY NETWORK

Here, we derive two asymptotic OP cases for the SN. In Case 1, we assume that the SN is not restricted by the ITC level. Therefore, considering $I_{\text{ITC}} \to \infty$, $\gamma_{R,b}$ in (13) can be rewritten as

$$\begin{aligned} F_{\gamma_{R,b}}^{[1]}(\psi_j) &= \Pr[X < Z\mathcal{K} + \mathcal{M} + \mathcal{L}] \\ &= \int_0^{\infty} f_Z(z) F_X(z\mathcal{K} + \mathcal{M} + \mathcal{L}) \text{d}z \\ &= \int_0^{\infty} e^{-z} \left(1 - e^{-Z\mathcal{K} - \mathcal{M} - \mathcal{L}}\right) \text{d}z \\ &= 1 - \frac{e^{-\mathcal{M}-\mathcal{L}}}{1+\mathcal{K}}. \end{aligned} \quad (19)$$

The CDF of $\gamma_{b,b}$ in (15) can be derived using similar approach as for $\gamma_{R,b}$ and written as

$$F_{\gamma_{b,b}}^{[1]}(\psi_j) = 1 - \frac{e^{-\mathcal{O}-\mathcal{T}}}{1+\mathcal{S}}. \quad (20)$$

Then, by inserting (19) and (20) into (12), the OP for Case 1 can be written as

$$P_{\text{out}}^{b[1]} = 1 - \frac{e^{-\mathcal{M}-\mathcal{L}-\mathcal{O}-\mathcal{T}}}{(\mathcal{K}+1)(\mathcal{S}+1)}. \quad (21)$$

In Case 2, it is assumed that the ITC is the dominant factor in determining the maximum allowed transmit power at the SN. Hence, the CDF of $\gamma_{R,b}$ in (13) can be rewritten for Case 2 as

$$\begin{aligned} F_{\gamma_{R,b}}^{[2]}(\psi_j) &= \Pr\left[X < Z\overline{\mathcal{K}} + Y\overline{\mathcal{M}} + \mathcal{L}\right] \\ &= \int_0^{\infty} e^{-z} \int_0^{\infty} e^{-y} \left(1 - e^{-z\mathcal{K} - y\overline{\mathcal{M}} - \mathcal{L}}\right) \text{d}y\text{d}z \\ &= \int_0^{\infty} e^{-z} \text{d}z - e^{-\mathcal{L}} \int_0^{\infty} \frac{e^{-z}}{z\overline{\mathcal{K}} + \overline{\mathcal{M}} + 1} \text{d}z \\ &\overset{a}{=} 1 + \frac{e^{-\mathcal{L} + \frac{\overline{\mathcal{M}}+1}{\overline{\mathcal{K}}}} \text{Ei}\left[-\frac{\overline{\mathcal{M}}+1}{\overline{\mathcal{K}}}\right]}{\overline{\mathcal{K}}}, \end{aligned} \quad (22)$$

where a is obtained using [34, Eq. (3.352.4)]. Similarly, the CDF of $\gamma_{b,b}$ in (15) can be derived for Case 2 as

$$F_{\gamma_{b,b}}^{[2]}(\psi_j) = 1 + \frac{e^{-\mathcal{T} + \frac{\overline{\mathcal{O}}+1}{\overline{\mathcal{S}}}} \text{Ei}\left[-\frac{\overline{\mathcal{O}}+1}{\overline{\mathcal{S}}}\right]}{\overline{\mathcal{S}}}. \quad (23)$$

Finally, after inserting (22) and (23) into (12), the OP for Case 2 can be derived as

$$P_{\text{out}}^{b[2]} = 1 - \frac{e^{-\mathcal{L}-\mathcal{T} + \frac{\overline{\mathcal{M}}+1}{\overline{\mathcal{K}}} + \frac{\overline{\mathcal{O}}+1}{\overline{\mathcal{S}}}}}{\overline{\mathcal{K}}\overline{\mathcal{S}}} \times \text{Ei}\left[-\frac{\overline{\mathcal{M}}+1}{\overline{\mathcal{K}}}\right] \text{Ei}\left[-\frac{\overline{\mathcal{O}}+1}{\overline{\mathcal{S}}}\right]. \quad (24)$$

Diversity order characterizes the impact of fading and system parameters on the outage performance and is denoted as the negative slope of the OP versus SNR on a log-log scale [35]. In order to obtain the diversity order, we consider a high SNR approximated OP for the SN. Hence, we first apply the power series expansion of $e^{-t} = 1 - t + \frac{(-t)^2}{2!} + \frac{(-t)^3}{3!} \cdots + \frac{(-t)^n}{n!}$, which can be approximated as $e^{-t} = 1 - t$ at high-SNR, in (17). Therefore, we rewrite the OP in (17) as (25), shown at the bottom of the page.

Further, considering $P = P_S = P_R \to \infty$, we rewrite (25) as

$$P_{\text{out}}^{b,P\to\infty} = 1 - \frac{\text{Ei}\left[-\xi_S\right] \text{Ei}\left[-\xi_R\right] e^{\xi_S + \xi_R}}{\overline{\mathcal{K}}\overline{\mathcal{S}}}. \quad (26)$$

From (26), we can notice that the OP becomes independent of the transmit power when $P \to \infty$. From this observations, one can deduce that the slope of the OP curve is equal to zero, which is also demonstrated by the diversity order equation of

$$D_b = \lim_{P\to\infty} \frac{-\log\left(P_{\text{out}}^{b,P\to\infty}\right)}{\log(P)}$$

$$P_{\text{out}}^{b} = 1 - \left(\frac{\Lambda_S(1 - \mathcal{M} - \mathcal{L})}{\mathcal{K}+1} - \frac{\text{Ei}\left[-\mu_S \xi_S\right] e^{\mu_S \xi_S}}{\overline{\mathcal{K}}} (1 - \Lambda_S\left(1 + \overline{\mathcal{M}}\right) - \mathcal{L}) \right) \times \left(\frac{\Lambda_R(1 - \mathcal{O} - \mathcal{T})}{\mathcal{S}+1} - \frac{\text{Ei}\left[-\mu_R \xi_R\right] e^{\mu_R \xi_R}}{\overline{\mathcal{S}}} (1 - \Lambda_R\left(1 + \overline{\mathcal{O}}\right) - \mathcal{T}) \right) \quad (25)$$

$$= \lim_{P\to\infty} \frac{-\log\left(1-\frac{\mathrm{Ei}[-\xi_S]\mathrm{Ei}[-\xi_R]e^{\xi_S+\xi_R}}{\bar{\mathcal{K}}\bar{\mathcal{S}}}\right)}{\log(P)} = 0. \quad (27)$$

C. OUTAGE FOR PRIMARY NETWORK

Similar to the SUs, the SIDNR to detect a primary signal x_T at D in the first time slot can be written as

$$\gamma_D = \frac{|h_{TD}|^2}{\phi_{TD}^2|h_{TD}|^2 + C_D + I_{SD}|g_{SD}|^2 + \delta_D}, \quad (28)$$

where the channel error plus hardware distortion noise power is given by $C_D = \zeta_{TD} + \zeta_{TD}\phi_{TD}^2$; the interference received from S is denoted by $I_{SD} = \frac{P_S}{P_T d_{SD}^{\tau}}(1+\phi_{SD}^2)$; and $\delta_D = \frac{\sigma_D^2}{P_T}$ is the normalized thermal noise at D. Now, the OP of D can be derived from $P_{\text{out}}^D = \Pr[\gamma_D < \psi_D]$.

Proposition 2: The OP of D is written in its closed form as

$$P_{\text{out}}^D = 1 - e^{-\mathcal{H}-\mathcal{I}}\left(e^{-\Lambda_S-\bar{\mathcal{E}}} + \frac{1-e^{-\Lambda_S(\mathcal{E}+1)}}{\mathcal{E}+1}\right), \quad (29)$$

where $\mathcal{H} = \frac{\delta_D\psi_D}{1-\phi_{TD}^2\psi_D}$; $\mathcal{I} = \frac{C_D\psi_D}{1-\phi_{TD}^2\psi_D}$; $\mathcal{E} = \frac{I_{SD}\psi_D}{1-\phi_{TD}^2\psi_D}$; and $\bar{\mathcal{E}} = \frac{I_{\text{ITC}}(1+\phi_{SD}^2)\psi_D}{\bar{P}_T(1-\phi_{TD}^2\psi_D)}$.

Proof: The proof is relegated in Appendix B. ■

We omit the derivation of the OP of D in the second time slot as it can be calculated by following a similar approach shown in Appendix B.

Next, we calculate the *diversity order* for D by, first, applying the approximation of $e^{-t} = 1 - t$ and the high SNR approximation, i.e., $P_T \to \infty$ into (29). Then, the deduced OP of $P_{\text{out}}^{D,P_T\to\infty} = 1 - e^{-\mathcal{I}}$ is used to calculate the diversity order as

$$D_D = \lim_{P_T\to\infty} \frac{-\log\left(P_{\text{out}}^{D,P_T\to\infty}\right)}{\log(P_T)} = \lim_{P_T\to\infty} \frac{-\log\left(1-e^{-\mathcal{I}}\right)}{\log(P_T)} = 0. \quad (30)$$

Similarly to SUs, the OP of D becomes independent of the transmit power when $P_T \to \infty$ and the slope of the primary OP curve is equal to zero.

V. OPTIMAL POWER ALLOCATION

This section provides the optimal PA that provides a fair OP for all users considering the ITC constraint at both time slots. Therefore, we formulate the PA problem using the following algorithm

$$\mathbf{P}_1: \max_{\boldsymbol{\alpha}_b,\boldsymbol{\beta}_b,\omega} \ \omega$$
$$\text{s.t. } \mathrm{P}_1^1: \gamma_b \geq \omega, \ \forall b \in \{1,\ldots,B\}$$
$$\mathrm{P}_1^2: \sum \alpha_b \leq 1 \text{ and } \sum \beta_b \leq 1$$
$$\mathrm{P}_1^3: \alpha_b, \beta_b \in [0,1], \forall b \quad (31)$$

where $\boldsymbol{\alpha}_b = [\alpha_1,\ldots,\alpha_B]$ and $\boldsymbol{\beta}_b = [\beta_1,\ldots,\beta_B]$. In (31), we handle the max-min objective by setting the objective to an auxiliary variable ω and enforcing all SIDNRs to be not less than ω in P_1^1. Further, P_1^2 represents the maximum transmission PA factors on the first and second time slots. P_1^3 shows that the PA factors α_b and β_b take values from 0 to 1. We solve $\mathbf{P}_1$ numerically using geometric programming [36], where we alter P_1^1 into $1/\gamma_b \leq 1/\omega$ to put inequality constraints in the form of posynomials.

VI. SPECTRAL EFFICIENCY

This section analyses the SE of cooperative CR-NOMA networks by considering HI, imperfect CSI, ITC and SIC. Considering optimal power allocation factors obtained in Section V, we further provide upper bound and high-SNR asymptotic expressions for SE of U_b [4]

A. UPPER BOUND ON SPECTRAL EFFICIENCY

The SE is defined as the maximum achievable rate averaged over all fading states. The derivation of the exact SE is complex or even intractable due to the considered ITC and system imperfections. Hence, we provide the upper bound on SE, which tightly matches the exact Monte-Carlo simulated EC as will be shown in Section VII. The generic SE of U_b can be found as

$$\mathcal{C}_b = \frac{\mathcal{W}}{2}\mathbb{E}\{\log_2(1+\gamma_{b,b})\}. \quad (32)$$

Proposition 3: The upper bound on SE of U_b, considering system imperfections and the ITC, is written as in (33), at the bottom of the page.

Proof: See Appendix C. ■

B. HIGH-SNR ASYMPTOTIC SPECTRAL EFFICIENCY

In this part, we provide a high-SNR approximation for the SE of the proposed system model to provide a deeper insight. Hence, by taking the limit of SIDNR regarding the high transmission power, we rewrite (32) as

$$\mathcal{C}_b^{\text{HS}} = \frac{\mathcal{W}}{2}\mathbb{E}\left\{\log_2\left[1+\lim_{P_R\to\infty}\frac{\beta_b Q}{\mathcal{P}Q+C_b}\right]\right\} = \frac{\mathcal{W}}{2}\mathbb{E}\left\{\log_2\left[\frac{Q(\mathcal{P}+\beta_b)+C_b}{\mathcal{P}Q+C_b}\right]\right\}. \quad (34)$$

4. The max-min fair objective in Section V searches for the optimal power allocation factors aiming to equalize rates of broadcast and access links to the auxiliary rate variable ω. Doing so, it guarantees equal rate performance for both links. Therefore, we consider SIDNR of the access link to derive the SE.

$$\mathcal{C}_b = \left(1-e^{-\Lambda_R}\right)\left(\frac{\mathcal{W}}{2}\log_2[\mathcal{G}+C_b+I_{Tb}+\delta_b] - \frac{\mathcal{W}}{2}\log_2[\mathcal{P}+C_b+I_{Tb}+\delta_b]\right) + e^{-\Lambda_R}\left(\frac{\mathcal{W}}{2}\log_2\left[\mathcal{G}+C_b+\bar{I}_{Tb}+\bar{\delta}_b\right] - \frac{\mathcal{W}}{2}\log_2\left[\mathcal{P}+C_b+\bar{I}_{Tb}+\bar{\delta}_b\right]\right) \quad (33)$$

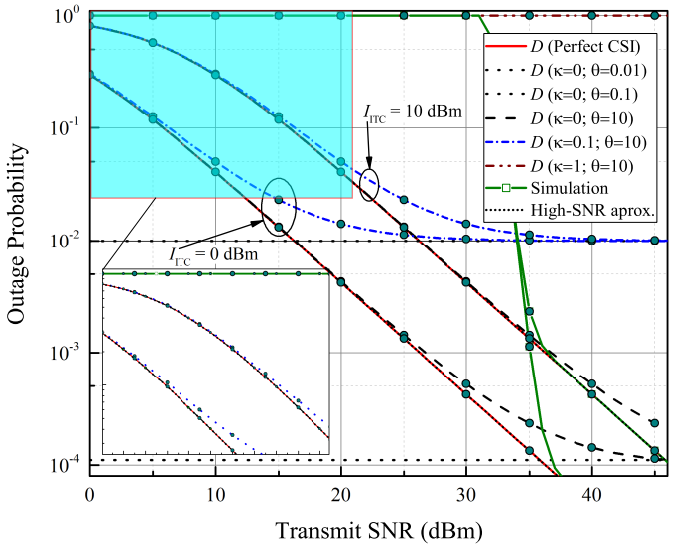

FIGURE 2. The OP versus the transmit SNR for the primary destination considering various channel uncertainties, $\phi = 0$ and $\vartheta = 0$.

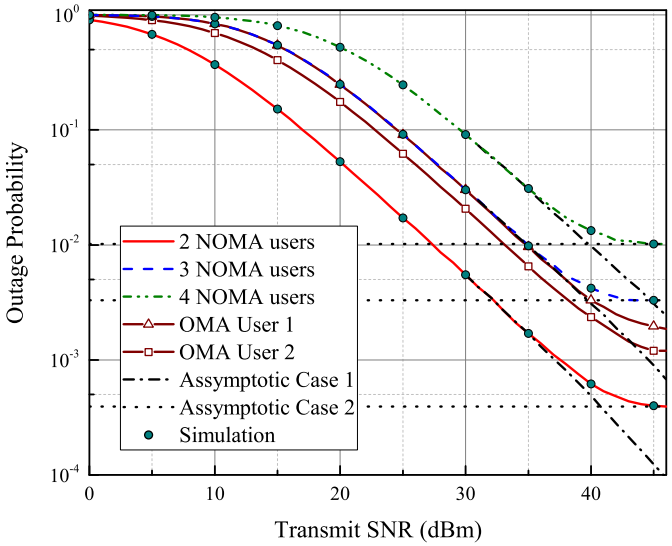

FIGURE 3. The OP versus the transmit SNR for OMA and NOMA users with $P_T = 30$ dBm, $I_{\text{ITC}} = 0$ dBm, $\zeta = 0$, $\phi = 0$ and $\vartheta = 0$.

Then, by using the property of a logarithm function, (34) can be further re-written as a difference of two terms as

$$\begin{aligned}\mathcal{C}_b^{\text{HS}} &= \frac{\mathcal{W}}{2}\mathbb{E}\{\log_2[T + C_b]\} - \frac{\mathcal{W}}{2}\mathbb{E}\{\log_2[V + C_b]\} \\ &= \frac{\mathcal{W}}{2}\underbrace{\int_0^\infty \log_2(t + C_b) f_T(t)\mathrm{d}t}_{\Omega_1} \\ &\quad - \frac{\mathcal{W}}{2}\underbrace{\int_0^\infty \log_2(v + C_b) f_V(v)\mathrm{d}v}_{\Omega_2}, \end{aligned} \tag{35}$$

where $T = Q(\mathcal{P} + \beta_b)$ and $V = \mathcal{P}Q$.

Proposition 4: The high-SNR asymptotic spectral efficiency of U_b is written in its closed-form as

$$\begin{aligned}\mathcal{C}_b^{\text{HS}} &= \frac{1}{\ln(2)} G_3^{1\ 3}_{2\ 2}\left(\frac{\mathcal{P} + \beta_b}{C_b}\middle| \begin{matrix}0, 1, 1\\ 1, 0\end{matrix}\right) \\ &\quad - \frac{1}{\ln(2)} G_3^{1\ 3}_{2\ 2}\left(\frac{\mathcal{P}}{C_b}\middle| \begin{matrix}0, 1, 1\\ 1, 0\end{matrix}\right). \end{aligned} \tag{36}$$

Proof: The proof is relegated in Appendix D. ■

VII. NUMERICAL RESULTS

This section discusses the numerical results and validates that all theoretical analyses precisely match the Monte-Carlo simulations with following system settings: the same transmit power at S and R; $\mathcal{R}_{\text{th},1} = \mathcal{R}_{\text{th},2} = 1$ bit/s/Hz [9]; similar distances as in [37] are taken as $d_{SR} = 50$ m; $d_{SD} = d_{RD} = 100$ m; $d_{TR} = d_{TB} = 200$ m; $\{d_{R1}, d_{R2}, d_{R3}, d_{R4}\} = \{75, 50, 25, 15\}$ m; $\mathcal{W} = 1$ Hz; $\tau = 3$ [7]; and $\sigma_j^2 = -174$ dBm/Hz [32], $\forall j \in \{R, D, b, \ldots, B\}$. Moreover, the parameters for imperfect CSI and hardware impairments follow the values in [20], [22], [27].

Fig. 2 shows the impact of the channel error variance on the outage performance of the primary destination in the first time slot. It is observed that the increase of an ITC level degrades the OP of D. For example, at 30 dBm transmit SNR, D obtains the OP of 4.2×10^{-4} and 4.2×10^{-3} when $I_{\text{ITC}} = 0$ dBm and $I_{\text{ITC}} = 10$ dBm, respectively. The OP degradation when the value of ITC is higher happens due to an increased level of interference from the SN. Further, the impact of channel uncertainty scenarios can be considered as follows. When $\kappa = 0$, the channel error variance becomes SNR-independent and increasing transmit SNR provides no advantage. However, the outage performance degrades by increasing θ. One observation is that when θ is small, it does not cause a considerable impact on the OP at lower SNR values. The reason is that, when θ tends to zero, the channel estimation approaches the perfect CSI. Hence, the effect of the small θ on the OP is imperceptible at lower SNRs. For instance, when $I_{\text{ITC}} = 0$ dBm and transmit SNR of 25 dBm, the achievable OP for $\{k = 0;\ \theta = 0.01\}$ is 1.4×10^{-3}, which is a very tight result to the perfect-case OP curve. However, the OP curve for the channel imperfection of $\{k = 0; \theta = 0.1\}$ degrades to 1.2×10^{-2} compared to the perfect CSI scenario. On the other hand, when $\theta = 10$, D obtains full outage at all SNR values. When $\kappa \neq 0$, the OP saturation is not noticed as the channel error model becomes SNR-dependent, and the increase of κ results in an improvement of the OP as the channel error is inversely proportional to the SNR. For example, when $\kappa = 0.1$ and $\theta = 10$, we can see that the impact of channel error decreases after the transmit SNR of 32 and outage curves approach the performance of the perfect CSI at 37 dBm. Finally, when $\kappa = 1$, the system obtains the OP of the perfect case at low-SNR levels.

In Fig. 3, to demonstrate the impact of ITC on the OP of secondary users, we consider the asymptotic Cases 1 and 2 in Section IV-B. Here, we plot the OP results of two-, three-

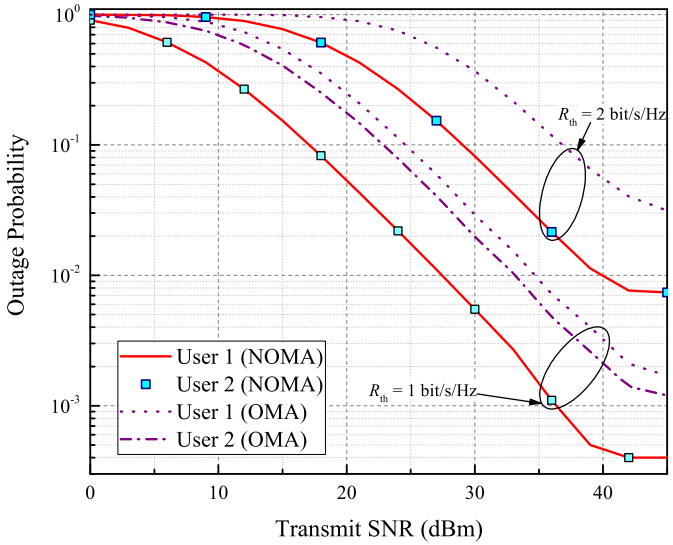

FIGURE 4. The OP versus the transmit SNR for the two-user NOMA and OMA scenarios with $P_T = 30$ dBm, $I_{\text{ITC}} = 0$ dBm.

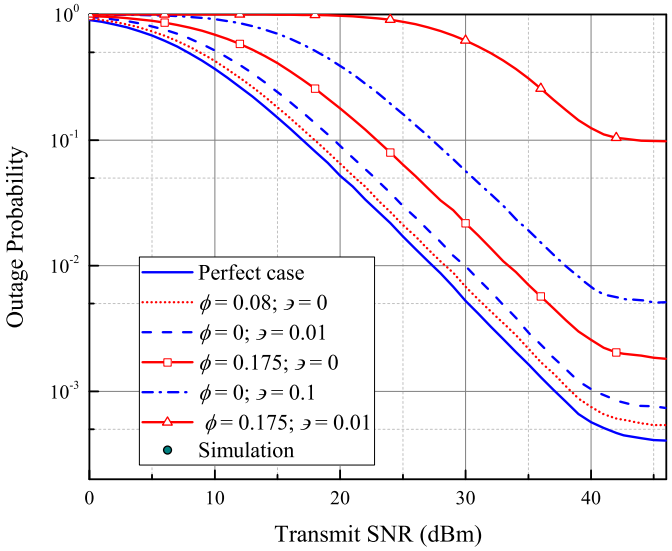

FIGURE 5. The OP versus the transmit SNR for the two-user NOMA scenario with $P_T = 30$ dBm, $I_{\text{ITC}} = 0$ dBm and $\zeta = 0$.

and four-user NOMA scenarios. The OP of users in each scenario is optimized solving $\mathbf{P}_1$ in Section V and all users obtain the same OP. It is noticed that the two-user NOMA scenario performs better than three- and four-user NOMA scenarios. Due to these results, it may not be feasible to consider many NOMA users as each user's OP degrades significantly. Moreover, we compare the OP of the two-user scenario operating on OMA and NOMA. For the sake of a fair comparison, the rate requirement of cooperative OMA is set as two-fold of that used for cooperative NOMA. It is noticed that NOMA users achieve a better OP than corresponding OMA users. Additionally, we can observe that the imposed ITC results in OP saturation. This implies that secondary transmitters cannot increase transmission power above the ITC level without causing harmful interference to D. Regarding Asymptotic cases 1 and 2, we can see that, in Case 1, the curves show the OP improvement at high transmit SNRs without outage saturation. Finally, in Case 2, where the maximum allowed transmit power of the source is restricted to the ITC value, we notice that the OP curves match with those of Case 1 at high SNR values.

In Fig. 4, we compare the performance of OMA and NOMA networks considering different rate thresholds. It is noticed that, when the rate requirements are set to $\mathcal{R}_{\text{th},1} = \mathcal{R}_{\text{th},2} = 1$ bit/s/Hz, NOMA users obtain better outage performance than OMA ones. Further, when we increase the date rate requirement for user 1 to $\mathcal{R}_{\text{th},1} = 2$ bit/s/Hz, NOMA users still perform better than OMA user 1; however, they are not superior to OMA user 2. This happens since the optimal power allocation algorithm provides fair/equal outage performance for both NOMA users. Therefore, higher power is allocated to NOMA user 1 due to its channel quality and date rate requirement, which leads to degradation of the overall optimal outage performance. From these results, it can be deduced that the proper rate threshold should be chosen for NOMA users to provide better results than OMA users.

Fig. 5 presents the impact of HIs and imperfect SIC on the OP of two-user NOMA scenario considering $\zeta = 0$. The plot shows that the imperfect SIC degrades the OP of NOMA users. For instance, at 30 dBm transmit SNR, users obtain the OP of 5.7×10^{-2} and 1×10^{-2} when $\vartheta = 0.01$ and $\vartheta = 0.1$, respectively, while the OP for perfect SIC is 5.3×10^{-3}. Here, we notice that the imperfect SIC of $\vartheta = 0.01$ degrades the OP for 10 times and the increase of the SIC imperfection causes further OP degradation. Additionally, we set two different HI levels[5] as $\phi = 0.08$ and $\phi = 0.175$ to show the effect of HIs on the system performance. At 30 transmit SNR, the OP of the system with settings $\phi = 0.08$ degrades to 6.8×10^{-3}, which not considerable outage degradation comparing to perfect outage curve. This result can state that a lower level of HI does not cause a substantial impact on the OP. However, when HI is increased to $\phi = 0.175$, we can see that the OP degrades to 2.2×10^{-2}, which shows that the impact of the HI is noticeable at high HI levels. Moreover, when both imperfections present, i.e., $\phi = 0.175$ and $\vartheta = 0.01$, the OP performance degrades significantly by showing the worst performance. i.e., the OP of 0.62 at 30 dBm transmit power.

The average throughput for the two-NOMA users scenario obtained from (18) is illustrated in Fig. 6. Similarly to the OP, the higher value of embedded ITC causes a saturation for the throughput curves at lower transmit SNR values. For instance, when $I_{\text{ITC}} = 0$ dBm, the throughput curves start saturating at 45 dBm, while saturation for the case with $I_{\text{ITC}} = -10$ dBm starts at 35 dBm. Moreover, when the

5. Regarding to [31], the practical values of ϕ is [0.08, 0.175].

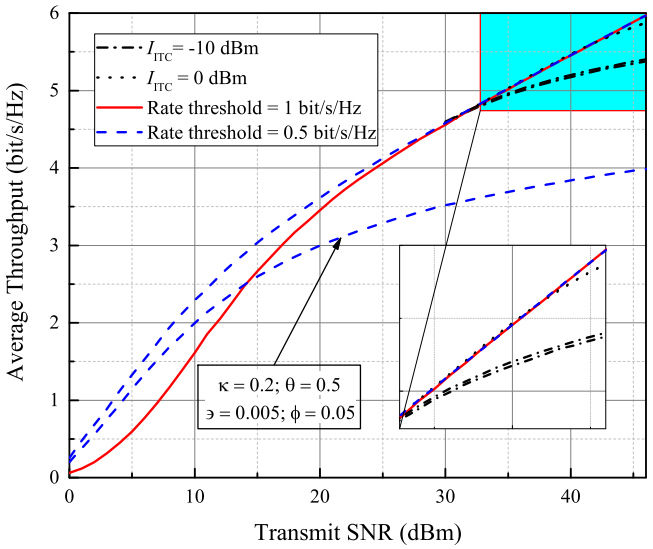

FIGURE 6. The average throughput versus the transmit SNR for the two-user NOMA scenario considering the perfect and imperfect models.

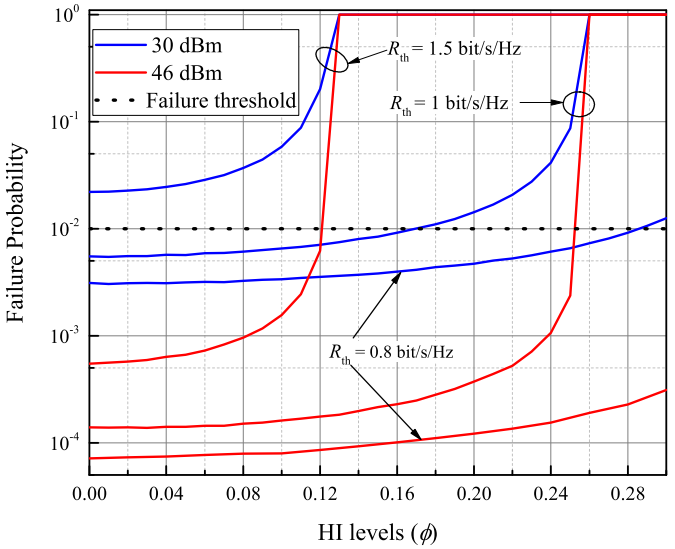

FIGURE 7. The failure probability versus the HI levels for the two-user NOMA scenario when $\zeta = 0$ and $\vartheta = 0$.

rate threshold $\mathcal{R}_{\text{th}} = 0.5$ bit/s/Hz, the throughput performs better comparing to the scenario with $\mathcal{R}_{\text{th}} = 1$ bit/s/Hz at lower and moderate transmit SNR values. However, NOMA users obtain the same throughput at high SNRs for the both rate thresholds. This means that the transmit SNR $>$ 30 dBm is enough to satisfy QoS for both considered rate thresholds. In addition, we notice that the compound effect of imperfect CSI, SIC and HI notably deteriorates the throughput performance by showing the worst throughput result among all curves. Furthermore, due to the condition of $\psi_b < \min(\frac{\alpha_b}{I_{Rb}+\phi^2_{SR}}, \frac{\beta_b}{I_{bb}+\phi^2_{Rb}})$ and depending on the level of hardware and SIC impairments, one needs to choose the value of the rate threshold properly in order to provide some tolerant OP or throughput level for NOMA users.

The design of a HI-free system in modern wireless networks is extremely costly and, for mmWave communication, this task becomes more challenging due to the scaling laws [38]. However, some wireless devices are tolerant to some level of HIs if their QoS is met. Hence, in Fig. 7, we present the HI level effect on the system failure. Here, we assume that the system has a failure probability threshold of 10^{-2}. In other words, we assume that the NOMA users are tolerant to outage probability of 10^{-2} and the communication fails if this condition is not satisfied. We consider 30 and 46 dBm transmission power and data rate thresholds set as $\mathcal{R}_{\text{th}} = \{0.8; 1; 1.5\}$ bit/s/Hz. As can be observed, the failure probability of the system increases with the higher level of HIs. It is worth mentioning that the failure probability also depends on the date rate requirement of the system. For example, when the transmit SNR is 30 dBm and $\mathcal{R}_{\text{th}} = 1.5$ bit/s/Hz, the system can not attain failure threshold and declares failure in all HIs values. On the other hand, when $\mathcal{R}_{\text{th}} = 1$ bit/s/Hz, the system faces failure at the HI level of 0.13, while, the failure happens

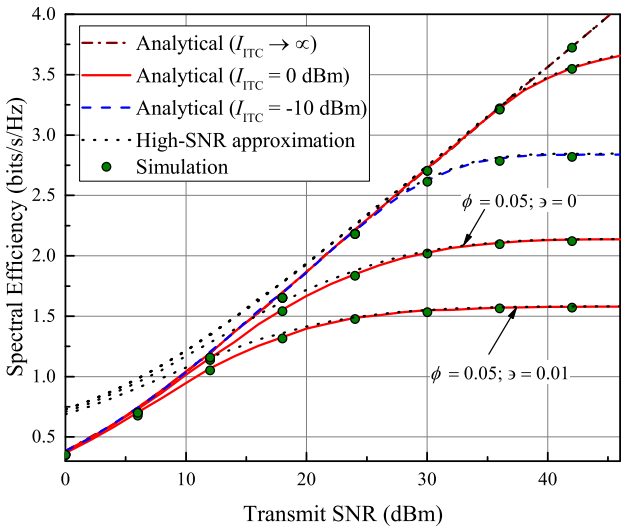

FIGURE 8. The SE versus the transmit SNR for two-user scenario considering system imperfections.

at the HI value of 0.29 when $\mathcal{R}_{\text{th}} = 0.8$ bit/s/Hz. This means that, besides the HIs level, it is also crucial to choose the date rate threshold properly to provide failure-free communication. In addition, an increase of the transmit SNR to 46 dBm shows more HIs-tolerant performance. For instance, when $\mathcal{R}_{\text{th}} = 1.5$ bit/s/Hz and $\mathcal{R}_{\text{th}} = 1$ bit/s/Hz, the system demonstrates error-tolerance up to HIs levels of 0.12 and 0.25, respectively. Also, considering the same system settings with $\mathcal{R}_{\text{th}} = 0.8$ bit/s/Hz, the system declares no failure for the considered HI levels.

In Fig. 8, we present the results for the SE derived in Section VI considering the system imperfections and the two-user case scenario. Two NOMA users provide the same SE performance due to the optimal PA strategy proposed in

Section V. Hence, the results in the plot are related to both users. First of all, it is worth mentioning that the upper bound on SE provides tight agreement with the simulated exact SE. Moreover, high-SNR approximation results coincide with the exact and upper bound SE results after 27 dBm transmit SNR. These results validate the derived SE equations' correctness, which can be alternatively used to analyze the exact SE performance accurately. Furthermore, it is noticed that the system imperfections cause SE at high SNR regions. For example, when $\phi = 0.05$ and $\ni = 0$, the curve of the SE saturates after 30 dBm transmit SNR and obtains the maximum SE of 2.2 bits/s/Hz, which is almost half value of the ideal SE ($I_{\text{ITC}} \to \infty$) at 46 dBm transmit SNR. In addition, when $\phi = 0.05$ and $\ni = 0.01$, the addition of SIC imperfection results in a worse capacity performance by receiving the maximum SE of 1.65 bits/s/Hz.

VIII. CONCLUSION

This paper analyzed the performance of the downlink underlay CR-NOMA DF-based relaying network considering practical system constraints such as hardware, CSI, and SIC imperfections. Exact and analytical closed-form expressions for the end-to-end OP of primary and secondary users were derived considering inter-network interference. Besides, several useful insights on the system performance were derived by obtaining approximated closed-form OP expressions. We drew the results on the single and joint effect of system imperfections on system performance. As a result, it can be concluded that the increase of the level of system imperfections, i.e., HIs, imperfect CSI and SIC, leads to the outage degradation or full outage of CR-NOMA networks. Moreover, this study's results underline the importance of considering HIs present at transceivers when applications with strict reliability conditions are considered. The results suggest that the effect of HIs on the OP enhances with the increase of the rate threshold. Furthermore, we provided the mathematically tractable upper bound on SE and its high-SNR approximation that provide valuable insights into the effect of each system impairment. Moreover, we proposed the optimal PA model to guarantee outage fairness among NOMA users. The proposed NOMA system model obtained better OP results than the OMA one, which is considered as a benchmark model. Finally, the accurateness of the derived analytical expressions was verified by Monte Carlo simulations.

APPENDIX A
PROOF OF PROPOSITION 1

The term Δ in (13) can be derived as

$$\begin{aligned}\Delta &= \int_{z=0}^{\infty} f_Z(z) \int_{x=0}^{z\mathcal{K}+\mathcal{M}+\mathcal{L}} f_X(x)\mathrm{d}x\mathrm{d}z \int_{y=0}^{\Lambda_S} f_Y(y)\mathrm{d}y \\ &= \left(1-e^{-\Lambda_S}\right)\int_{z=0}^{\infty} e^{-z}\left(1-e^{-(z\mathcal{K}+\mathcal{M}+\mathcal{L})}\right)\mathrm{d}z \\ &= \left(1-e^{-\Lambda_S}\right)\left(1-\frac{e^{-(\mathcal{M}+\mathcal{L})}}{1+\mathcal{K}}\right). \end{aligned} \tag{1.1}$$

Then, the term Υ in (13) can be rewritten as follows

$$\Upsilon = \int_{z=0}^{\infty} f_Z(z) \underbrace{\int_{y=\Lambda_S}^{\infty}\int_{x=0}^{z\mathcal{y}\overline{\mathcal{K}}+y\overline{\mathcal{M}}+\mathcal{L}} f_Y(y)f_X(x)\mathrm{d}x\mathrm{d}y}_{\Upsilon_1}\mathrm{d}z, \tag{1.2}$$

while the term Υ_1 in (1.2) can be derived as

$$\begin{aligned}\Upsilon_1 &= \int_{y=\Lambda_S}^{\infty} e^{-y}\left(1-e^{-\left(z\mathcal{y}\overline{\mathcal{K}}+y\overline{\mathcal{M}}+\mathcal{L}\right)}\right)\mathrm{d}y \\ &= e^{-\Lambda_S} - \frac{e^{-\mathcal{L}}\ e^{-\Lambda_S\left(z\overline{\mathcal{K}}+\overline{\mathcal{M}}+1\right)}}{z\overline{\mathcal{K}}+\overline{\mathcal{M}}+1}. \end{aligned} \tag{1.3}$$

Then, by inserting (1.3) into (1.2), we can rewrite Υ by

$$\begin{aligned}\Upsilon = &\int_{z=0}^{\infty} e^{-z}\ e^{-\Lambda_S}\mathrm{d}z - \frac{e^{-\mathcal{L}-\Lambda_S\overline{\mathcal{M}}-\Lambda_S}}{\overline{\mathcal{K}}} \\ &\times \int_{z=0}^{\infty} \frac{e^{-z\left(1+\Lambda_S\overline{\mathcal{K}}\right)}}{z+\frac{\overline{\mathcal{M}}+1}{\overline{\mathcal{K}}}}\mathrm{d}z. \end{aligned} \tag{1.4}$$

Now, by using [34, Eq. (3.352.4)], the term Υ can be derived in a closed-form as

$$\Upsilon = e^{-\Lambda_S} + \frac{e^{-\left(\mathcal{L}+\Lambda_S\overline{\mathcal{M}}\right)-\Lambda_S}}{\overline{\mathcal{K}}} e^{\mu_S\xi_S}\mathrm{Ei}\left[-\mu_S\xi_S\right]. \tag{1.5}$$

Finally, by inserting (1.1) and (1.5) into (13), the closed-form expression for the CDF of $\gamma_{R,b}$ can be written as in (14), where $\psi_b < \frac{\alpha_b}{I_{Rb}+\phi_{SR}^2}$; otherwise, $F_{\gamma_{R,b}}(\psi_b) \approx 1$.

APPENDIX B
PROOF OF PROPOSITION 2

Considering the ITC applied at D, the CDF of the RV γ_D can be written as

$$\begin{aligned}P_{\text{out}}^{D} &= \Pr\left[\frac{V}{\phi_{TD}^2 V + C_D + I_{SD}Y + \delta_D} < \psi_D,\ Y < \Lambda_S\right] \\ &\quad + \Pr\left[\frac{V}{\phi_{TD}^2 V + C_D + \frac{I_{\text{ITC}}(1+\phi_{SD}^2)}{P_T} + \delta_D} < \psi_D,\ Y > \Lambda_S\right] \\ &= \underbrace{\Pr[V < Y\mathcal{E}+L, Y < \Lambda_S]}_{A} + \underbrace{\Pr[V < \overline{\mathcal{E}}+L, Y > \Lambda_S]}_{B}, \end{aligned} \tag{2.1}$$

where $L = \mathcal{H} + \mathcal{I}$. The terms A and B in (2.1) can be respectively further derived as

$$\begin{aligned}A &= \int_{y=0}^{\Lambda_S} f_Y(y)F_V(v)\mathrm{d}y = \int_{y=0}^{\Lambda_S} e^{-y}\left(1-e^{-(y\mathcal{E}+L)}\right)\mathrm{d}y \\ &= 1 - e^{-\Lambda_S} - \frac{1-e^{-\Lambda_S(\mathcal{E}+1)}}{\mathcal{E}+1}e^{-L}, \end{aligned} \tag{2.2}$$

$$B = F_V(v)\int_{y=\Lambda_S}^{\infty} f_Y(y)\mathrm{d}y = e^{-\Lambda_S}\left(1-e^{-(\overline{\mathcal{E}}+L)}\right). \tag{2.3}$$

Finally, the OP of U_D can be derived after substituting (2.2) and (2.3) into (2.1) and written as in (29).

APPENDIX C
PROOF OF PROPOSITION 3

By using (8) and considering the ITC, we further extend (32) as in (3.1), at the bottom of the page where $\mathbb{E}\{\cdot\}$ is the expectation operator, L_1 is the probability that P_R is less than the ITC level, while Φ_1 is the corresponding SE for this scenario. Moreover, L_2 denotes the probability that P_S exceeds the ITC level with the SE of Φ_2.

The term L_1 in (3.1) can be derived as

$$L_1 = \Pr(Y < \Lambda_R) = \int_0^{\Lambda_R} e^{-y}\mathrm{d}y = 1 - e^{-\Lambda_R}. \quad (3.2)$$

The term Φ_1, by using the property of a logarithm function, can be further re-written as a difference of two terms as

$$\Phi_1 = \frac{\mathcal{W}}{2}\mathbb{E}\big\{\log_2[\mathcal{G}Q + C_b + I_{Tb}W + \delta_b]\big\} - \frac{\mathcal{W}}{2}\mathbb{E}\big\{\log_2[\mathcal{P}Q + C_b + I_{Tb}W + \delta_b]\big\}, \quad (3.3)$$

where $\mathcal{G} = \beta_b + I_{bb} + \phi_{Rb}^2$ and $\mathcal{P} = I_{bb} + \phi_{Rb}^2$. Now, considering that a logarithm is a concave function, we apply Jensen's inequality to evaluate the upper bound on SE as

$$\begin{aligned}\Phi_1 &\le \frac{\mathcal{W}}{2}\big\{\log_2[\mathcal{G}\mathbb{E}\{Q\} + C_b + I_{Tb}\mathbb{E}\{W\} + \delta_b]\big\} - \frac{\mathcal{W}}{2}\big\{\log_2[\mathcal{P}\mathbb{E}\{Q\} + C_b + I_{Tb}\mathbb{E}\{W\} + \delta_b]\big\} \\ &\le \frac{\mathcal{W}}{2}\big\{\log_2[\mathcal{G} + C_b + I_{Tb} + \delta_b]\big\} - \frac{\mathcal{W}}{2}\big\{\log_2[\mathcal{P} + C_b + I_{Tb} + \delta_b]\big\}, \end{aligned} \quad (3.4)$$

where $\mathbb{E}\{Q\} = \int_0^\infty q f_Q(q)\mathrm{d}q = \int_0^\infty q e^{-q}\mathrm{d}q = 1$ and $\mathbb{E}\{W\} = \int_0^\infty w e^{-w}\mathrm{d}w = 1$.

The term L_2 in (3.1) can be derived as

$$L_2 = \Pr(Y > \Lambda_R) = \int_{\Lambda_R}^\infty e^{-y}\mathrm{d}y = e^{-\Lambda_R}. \quad (3.5)$$

Similarly to Φ_1, the term Φ_2 in (3.1) can be calculated as

$$\Phi_2 \le \frac{\mathcal{W}}{2}\big\{\log_2\big[\mathcal{G}\mathbb{E}\{Q\} + C_b + \bar{I}_{Tb}\mathbb{E}\{WY\} + \bar{\delta}_b\mathbb{E}\{Y\}\big]\big\} - \frac{\mathcal{W}}{2}\big\{\log_2\big[\mathcal{P}\mathbb{E}\{Q\} + C_b + \bar{I}_{Tb}\mathbb{E}\{WY\} + \bar{\delta}_b\mathbb{E}\{Y\}\big]\big\}, \quad (3.6)$$

where $\mathbb{E}\{Y\} = \int_0^\infty y e^{-y}\mathrm{d}y = 1$. In order to derive $\mathbb{E}\{WY\}$ in (3.6), we first denote $T = WY$ and find the probability density functions (PDF) of new RV by using the rule of product of RVs as

$$\begin{aligned} f_T(t) &= \int_0^\infty \frac{1}{|w|} f_W(w) f_Y\Big(\frac{t}{w}\Big)\mathrm{d}w \\ &= \int_0^\infty \frac{1}{|w|} e^{-w} e^{-\frac{t}{w}}\mathrm{d}w = 2K_0\big(2\sqrt{t}\big), \end{aligned} \quad (3.7)$$

where $K_0(\cdot)$ is the modified Bessel function of second kind and zero order [34]. Now, we derive the expectation of T as

$$\mathbb{E}\{T\} = \mathbb{E}\{WY\} = \int_0^\infty 2t\,K_0\big(2\sqrt{t}\big)\mathrm{d}t = 1. \quad (3.8)$$

Then, Φ_2 can be further rewritten as

$$\Phi_2 \le \frac{\mathcal{W}}{2}\log_2\big[\mathcal{G} + C_b + \bar{I}_{Tb} + \bar{\delta}_b\big] - \frac{\mathcal{W}}{2}\log_2\big[\mathcal{P} + C_b + \bar{I}_{Tb} + \bar{\delta}_b\big]. \quad (3.9)$$

Finally, inserting (3.2), (3.4), (3.5) and (3.9) into (3.1), the upper bound on the SE for U_b can be written as (33).

APPENDIX D
PROOF OF PROPOSITION 4

First, to derive the integral Ω_1 in (35), we write the PDF of the RV T as $f_T(t) = \frac{1}{\mathcal{P}+\beta_b} e^{-\frac{t}{\mathcal{P}+\beta_b}}$ and re-express Ω_1 as

$$\Omega_1 = \frac{\ln(C_b)}{\ln(2)} + \frac{1}{\ln(2)\big(\mathcal{P}+\beta_b\big)} \times \underbrace{\int_0^\infty \ln\Big(1 + \frac{t}{C_b}\Big) e^{-\frac{t}{\mathcal{P}+\beta_b}}\mathrm{d}t}_{L}. \quad (4.1)$$

Now, applying following representations from [39, Eq. (11)] into terms L in the above equation, we can reformulate L as

$$\begin{aligned} L &= \int_0^\infty G_{0\,1}^{1\,0}\Big(\frac{t}{\mathcal{P}+\beta_b}\Big|\begin{matrix}-\\0\end{matrix}\Big) G_{2\,2}^{1\,2}\Big(\frac{t}{C_b}\Big|\begin{matrix}1,1\\1,0\end{matrix}\Big)\mathrm{d}t \\ &\overset{a}{=} (\mathcal{P}+\beta_b) G_{3\,2}^{1\,3}\Big(\frac{\mathcal{P}+\beta_b}{C_b}\Big|\begin{matrix}0,1,1\\1,0\end{matrix}\Big), \end{aligned} \quad (4.2)$$

where the terms a is derived using [34, Eq. (7.811.1)]. Further, inserting (4.2) into (4.1), Ω_1 is reformulated as follows

$$\Omega_1 = \frac{\ln(C_b)}{\ln(2)} + \frac{1}{\ln(2)} G_{3\,2}^{1\,3}\Big(\frac{\mathcal{P}+\beta_b}{C_b}\Big|\begin{matrix}0,1,1\\1,0\end{matrix}\Big). \quad (4.3)$$

$$C_b = \underbrace{\Pr(Y < \Lambda_R)}_{L_1}\underbrace{\frac{\mathcal{W}}{2}\mathbb{E}\left\{\log_2\left[1 + \frac{\beta_b Q}{(I_{bb} + \phi_{Rb}^2)Q + C_b + I_{Tb}W + \delta_b}\right]\right\}}_{\Phi_1} + \underbrace{\Pr(Y > \Lambda_R)}_{L_2}\underbrace{\frac{\mathcal{W}}{2}\mathbb{E}\left\{\log_2\left[1 + \frac{\beta_b Q}{(I_{bb} + \phi_{Rb}^2)Q + C_b + \bar{I}_{Tb}WY + \bar{\delta}_b Y}\right]\right\}}_{\Phi_2} \quad (3.1)$$

Using the pdf of $f_V(v) = \frac{1}{\mathcal{P}} e^{-\frac{v}{\mathcal{P}}}$ and similar approach in (4.1)-(4.2), the term Ω_2 in (35) can be derived as

$$\Omega_2 = \frac{\ln(C_b)}{\ln(2)} + \frac{1}{\ln(2)} G_3^{1\ 3}_{2\ 2}\left(\frac{\mathcal{P}}{C_b} \middle| \begin{matrix} 0, 1, 1 \\ 1, 0 \end{matrix} \right). \tag{4.4}$$

Finally, inserting (4.3) and (4.4) into (35), the high-SNR approximated spectral efficiency can be written as in (36).

REFERENCES

[1] J. Reed, M. Vassiliou, and S. Shah, "The role of new technologies in solving the spectrum shortage [point of view]," *Proc. IEEE*, vol. 104, no. 6, pp. 1163–1168, Jun. 2016.

[2] Y. Akhmetkaziyev *et al.*, "Performance of NOMA-enabled cognitive satellite-terrestrial networks with non-ideal system limitations," *IEEE Access*, vol. 9, pp. 35932–35946, 2021.

[3] L. Lv, J. Chen, Q. Ni, and Z. Ding, "Design of cooperative non-orthogonal multicast cognitive multiple access for 5G systems: User scheduling and performance analysis," *IEEE Trans. Commun.*, vol. 65, no. 6, pp. 2641–2656, Jun. 2017.

[4] S. Arzykulov *et al.*, "Hardware-and interference-limited cognitive IoT relaying NOMA networks with imperfect SIC over generalized non-homogeneous fading channels," *IEEE Access*, vol. 8, pp. 72942–72956, 2020.

[5] A. Celik and A. E. Kamal, "Green cooperative spectrum sensing and scheduling in heterogeneous cognitive radio networks," *IEEE Trans. Cogn. Commun. Netw.*, vol. 2, no. 3, pp. 238–248, Sep. 2016.

[6] Z. Ding *et al.*, "Application of non-orthogonal multiple access in LTE and 5G networks," *IEEE Commun. Mag.*, vol. 55, no. 2, pp. 185–191, Feb. 2017.

[7] Z. Yang, Z. Ding, P. Fan, and G. K. Karagiannidis, "On the performance of non-orthogonal multiple access systems with partial channel information," *IEEE Trans. Commun.*, vol. 64, no. 2, pp. 654–667, Feb. 2016.

[8] Y. Liu, Z. Ding, M. Elkashlan, and J. Yuan, "Nonorthogonal multiple access in large-scale underlay cognitive radio networks," *IEEE Trans. Veh. Technol.*, vol. 65, no. 12, pp. 10152–10157, Dec. 2016.

[9] L. Lv, Q. Ni, Z. Ding, and J. Chen, "Application of non-orthogonal multiple access in cooperative spectrum-sharing networks over Nakagami-*m* fading channels," *IEEE Trans. Veh. Technol.*, vol. 66, no. 6, pp. 5506–5511, Jun. 2017.

[10] Y. Chen, L. Wang, and B. Jiao, "Cooperative multicast non-orthogonal multiple access in cognitive radio," in *Proc. IEEE Int. Conf. Commun. (ICC)*, May 2017, pp. 1–6.

[11] J. Si, Z. Li, X. Chen, B. Hao, and Z. Liu, "On the performance of cognitive relay networks under primary user's outage constraint," *IEEE Commun. Lett.*, vol. 15, no. 4, pp. 422–424, Apr. 2011.

[12] S. Kim, W. Choi, Y. Choi, J. Lee, Y. Han, and I. Lee, "Downlink performance analysis of cognitive radio based cellular relay networks," in *Proc. 3rd Int. Conf. Cogn. Radio Orient. Wireless Netw. Commun. (CrownCom)*, May 2008, pp. 1–6.

[13] V. Kumar *et al.*, "Fundamental limits of spectrum sharing for NOMA-based cooperative relaying under a peak interference constraint," *IEEE Trans. Commun.*, vol. 67, no. 12, pp. 8233–8246, Dec. 2019.

[14] M. Jia *et al.*, "Performance analysis of cooperative non-orthogonal multiple access based on spectrum sensing," *IEEE Trans. Veh. Technol.*, vol. 68, no. 7, pp. 6855–6866, Jul. 2019.

[15] S. Arzykulov, G. Nauryzbayev, T. A. Tsiftsis, B. Maham, M. S. Hashmi, and K. M. Rabie, "Underlay spectrum sharing for NOMA relaying networks: Outage analysis," in *Proc. Int. Conf. Comput. Netw. Commun. (ICNC)*, 2020, pp. 897–901.

[16] X. Wang *et al.*, "Full-duplex relaying cognitive radio network with cooperative nonorthogonal multiple access," *IEEE Syst. J.*, vol. 13, no. 4, pp. 3897–3908, Dec. 2019.

[17] X. Yue, Y. Liu, Y. Yao, X. Li, R. Liu, and A. Nallanathan, "Secure communications in a unified non-orthogonal multiple access framework," *IEEE Trans. Wireless Commun.*, vol. 19, no. 3, pp. 2163–2178, Mar. 2020.

[18] H. Lei, R. Gao, K. Park, I. S. Ansari, K. J. Kim, and M. Alouini, "On secure downlink NOMA systems with outage constraint," *IEEE Trans. Commun.*, vol. 68, no. 12, pp. 7824–7836, Dec. 2020.

[19] V. Kumar, Z. Ding, and M. F. Flanagan, "On the performance of downlink NOMA in underlay spectrum sharing," *IEEE Trans. Veh. Technol.*, vol. 70, no. 5, pp. 4523–4540, May 2021.

[20] L. Tlebaldiyeva, B. Maham, and T. A. Tsiftsis, "Device-to-device mmWave communication in the presence of interference and hardware distortion noises," *IEEE Commun. Lett.*, vol. 23, no. 9, pp. 1607–1610, Sep. 2019.

[21] E. Björnson, J. Hoydis, M. Kountouris, and M. Debbah, "Massive MIMO systems with non-ideal hardware: Energy efficiency, estimation, and capacity limits," *IEEE Trans. Inf. Theory*, vol. 60, no. 11, pp. 7112–7139, Nov. 2014.

[22] E. Björnson, P. Zetterberg, M. Bengtsson, and B. Ottersten, "Capacity limits and multiplexing gains of MIMO channels with transceiver impairments," *IEEE Commun. Lett.*, vol. 17, no. 1, pp. 91–94, Jan. 2013.

[23] B. Selim, S. Muhaidat, P. C. Sofotasios, A. Al-Dweik, B. S. Sharif, and T. Stouraitis, "Radio-frequency front-end impairments: Performance degradation in nonorthogonal multiple access communication systems," *IEEE Veh. Technol. Mag.*, vol. 14, no. 1, pp. 89–97, Mar. 2019.

[24] X. Li, J. Li, Y. Liu, Z. Ding, and A. Nallanathan, "Residual transceiver hardware impairments on cooperative NOMA networks," *IEEE Trans. Wireless Commun.*, vol. 19, no. 1, pp. 680–695, Jan. 2020.

[25] S. Arzykulov, G. Nauryzbayev, T. Tsiftsis, and M. Abdallah, "Outage performance of cooperative underlay CR-NOMA with imperfect CSI," *IEEE Commun. Lett.*, vol. 23, no. 1, pp. 176–179, Jan. 2019.

[26] S. Arzykulov, G. Nauryzbayev, T. Tsiftsis, B. Maham, and M. Abdallah, "On the outage of underlay CR-NOMA networks with detect-and-forward relaying," *IEEE Trans. Cogn. Commun. Netw.*, vol. 5, no. 3, pp. 795–804, Sep. 2019.

[27] G. Nauryzbayev and E. Alsusa, "Interference alignment cancellation in compounded MIMO broadcast channels with general message sets," *IEEE Trans. Commun.*, vol. 63, no. 10, pp. 3702–3712, Oct. 2015.

[28] Z. Ding, M. Peng, and H. V. Poor, "Cooperative non-orthogonal multiple access in 5G systems," *IEEE Commun. Lett.*, vol. 19, no. 8, pp. 1462–1465, Aug. 2015.

[29] Z. Ding *et al.*, "Relay selection for cooperative NOMA," *IEEE Wireless Commun. Lett.*, vol. 5, no. 4, pp. 416–419, Aug. 2016.

[30] Z. Ding, L. Dai, and H. V. Poor, "MIMO-NOMA design for small packet transmission in the Internet of Things," *IEEE Access*, vol. 4, pp. 1393–1405, 2016.

[31] S. Sesia, I. Toufik, and M. Baker, *LTE—The UMTS Long Term Evolution: From Theory to Practice*, 2nd ed. New York, NY, USA: Wiley, 2011.

[32] M. Zeng *et al.*, "Power minimization for multi-cell uplink NOMA with imperfect SIC," *IEEE Wireless Commun. Lett.*, vol. 9, no. 12, pp. 2030–2034, Dec. 2020.

[33] F. Kara and H. Kaya, "Error probability analysis of NOMA-based diamond relaying network," *IEEE Trans. Veh. Technol.*, vol. 69, no. 2, pp. 2280–2285, Feb. 2020.

[34] I. S. Gradshteyn and I. M. Ryzhik, *Table of Integrals, Series, and Products*, 7th ed. Amsterdam, The Netherlands: Elsevier, 2007.

[35] E. Biglieri, R. Calderbank, A. Constantinides, A. Goldsmith, A. Paulraj, and H. V. Poor, *MIMO Wireless Communications*. Cambridge, MA, USA: Cambridge Univ. Press, 2010.

[36] S. Boyd *et al.*, "A tutorial on geometric programming," *Optim. Eng.*, vol. 8, no. 1, p. 67, 2007.

[37] A. V and B. Av, "Performance analysis of NOMA-based underlay cognitive radio networks with partial relay selection," *IEEE Trans. Veh. Technol.*, vol. 70, no. 5, pp. 4615–4630, May 2021.

[38] M. S. Khairy, A. Khajeh, A. M. Eltawil, and F. J. Kurdahi, "Equi-noise: A statistical model that combines embedded memory failures and channel noise," *IEEE Trans. Circuits Syst. I, Reg. Papers*, vol. 61, no. 2, pp. 407–419, Feb. 2014.

[39] V. S. Adamchik and O. I. Marichev, "The algorithm for calculating integrals of hypergeometric type functions and its realization in reduce system," in *Proc. Int. Symp. Symb. Algebraic Comput. (ISSAC)*, 1990, pp. 212–224. [Online]. Available: https://doi.org/10.1145/96877.96930

SULTANGALI ARZYKULOV (Member, IEEE) received the B.Sc. degree (Hons.) in radio engineering, electronics and telecommunications from Kazakh National Research Technical University after K. I. Satpayev, Almaty, Kazakhstan, in June 2010, the M.Sc. degree in communication engineering from the University of Manchester, Manchester, U.K., in 2013, and the Ph.D. degree in science, engineering and technology from Nazarbayev University, Nur-Sultan, Kazakhstan, in 2019, where he was a Postdoctoral Scholar from 2019 to 2020. He is currently a Postdoctoral Fellow with King Abdullah University of Science and Technology. His research interests include broad areas of wireless communication systems, with particular focus on intelligent reconfigurable surface, cognitive radio, energy harvesting, interference mitigation, and NOMA. He acts as a reviewer for several international journals/conferences and served as a technical program committee member on numerous IEEE Communication Society flagship conferences.

GALYMZHAN NAURYZBAYEV (Senior Member, IEEE) received the B.Sc. and M.Sc. (Hons.) degrees in radio engineering, electronics, and telecommunications from the Almaty University of Power Engineering and Telecommunication, Almaty, Kazakhstan, in 2009 and 2011, respectively, and the Ph.D. degree in wireless communications from the University of Manchester, U.K., in 2016. From 2016 to 2018, he held several academic and research positions with Nazarbayev University, Kazakhstan, L. N. Gumilyov Eurasian National University, Kazakhstan, and Hamad Bin Khalifa University, Qatar. In 2019, he joined Nazarbayev University as an Assistant Professor. His research interests are in the area of wireless communication systems, with particular focus on multiuser MIMO systems, cognitive radio, intelligent reconfigurable surface, signal processing, energy harvesting, visible light communications, NOMA, and interference mitigation. He served as a technical program committee member on numerous IEEE flagship conferences. He currently serves as a Member of the National Research Council of the Republic of Kazakhstan.

ABDULKADIR CELIK (Senior Member, IEEE) received the M.S. degree in electrical engineering, the M.S. degree in computer engineering, and the Ph.D. degree in co-majors of electrical engineering and computer engineering from Iowa State University, Ames, IA, USA, in 2013, 2015, and 2016, respectively. He was a Postdoctoral Fellow with the King Abdullah University of Science and Technology from 2016 to 2020, where he is currently a Research Scientist with the Communications and Computing Systems Lab. His research interests are in the areas of wireless communication systems and networks.

AHMED M. ELTAWIL (Senior Member, IEEE) received the B.Sc. and M.Sc. degrees (Hons.) from Cairo University, Giza, Egypt, in 1997 and 1999, respectively, and the Doctorate degree from the University of California at Los Angeles, Los Angeles, in 2003. He is a Professor with the Computer, Electrical and Mathematical Sciences and Engineering Division, King Abdullah University of Science and Technology (KAUST), which he joined in August 2019. Prior to that, he was a Professor with the Department of Electrical Engineering and Computer Science, University of California at Irvine, Irvine, in 2005. He is the Founder of the KAUST Communication and Computing System Laboratory, where he is pursuing research interests in the general area of low power digital circuit and signal processing architectures with an emphasis on mobile computing and communication systems and their applications, spanning wireless networks, personal networks and cyber-physical systems. He received several awards, as well as distinguished grants, including the NSF CAREER grant supporting his research in low power computing and communication systems, and the Henry Samueli School of Engineering, University of California at Irvine Innovator of the year award for 2021. He has been on the technical program committees and steering committees for workshops, symposia, and conferences in the areas of low power computing, wireless communication system design and CPS systems. He is a Senior Member of the National Academy of Inventors.